Check for updates

AGU100 ADVANCING EARTH AND SPACE SCIENCE

Geophysical Research Letters

RESEARCH LETTER
10.1029/2018GL077719

Key Points:
- Simulations of trends of noctilucent clouds (NLC) are studied on centennial timescales
- The visibility of NLC increases substantially due to water vapor increase, whereas cooling due to carbon dioxide increase has a negligible effect
- NLC presumably existed in historical times, but the chance to see them was extremely small

Correspondence to:
F.-J. Lübken,
luebken@iap-kborn.de

Citation:
Lübken, F.-J., Berger, U., & Baumgarten, G. (2018). On the anthropogenic impact on long-term evolution of noctilucent clouds. *Geophysical Research Letters*, *45*, 6681–6689. https://doi.org/10.1029/2018GL077719

Received 28 FEB 2018
Accepted 24 MAY 2018
Published online 2 JUL 2018

©2018. American Geophysical Union. All Rights Reserved.

On the Anthropogenic Impact on Long-Term Evolution of Noctilucent Clouds

Franz-Josef Lübken[1], Uwe Berger[1], and Gerd Baumgarten[1]

[1] Leibniz Institute of Atmospheric Physics, Kühlungsborn, Germany

Abstract Little is known about climate change effects in the transition region between the Earth's atmosphere and space, roughly at 80–120 km. Some of the earliest observations in this region come from *noctilucent clouds* (NLC) at ~83-km altitude. There is a long-standing dispute whether NLC are indicators of climate change. We use model simulations for a time period of 138 years to study the impact of increasing CO_2 and H_2O on the development of NLC on centennial time scales. Since the beginning of industrialization the water vapor concentration mixing ratio at NLC heights has increased by ~40% (1 ppmv) due to methane increase, whereas temperatures are nearly constant. The H_2O increase has led to a large enhancement of NLC brightness. NLC presumably existed centuries earlier, but the chance to observe them by the naked eye was extremely small before the twentieth century, whereas it is likely to see several NLC per season in the modern era.

Plain Language Summary In our paper we address a problem that is controversially disputed since several decades, namely, whether *noctilucent clouds* (NLC) in the middle atmosphere are indicators of climate change. NLC are a spectacular optical phenomenon in the summer season at midlatitudes. We show in our paper that (i) NLC are indeed indicators of anthropogenic activity, (ii) the reason for this is increasing water vapor (caused by methane increase), which significantly enhances the visibility of NLC; and (iii) contrary to common understanding, cooling of the middle atmosphere due to increased reduces(!) the visibility of NLC. NLC constitute the earliest observations in this height region. In our model we expose 40 million dust/ice particles to long-term changes in the middle atmosphere, namely, for 138 years starting with the beginning of industrialization. The model is nudged to the real world in the lower atmosphere. Since the beginning of industrialization,the chance to observe a bright NLC has increased from just one per several centuries(!) to a few per year. We conclude that NLC are indeed an indicator for climate change.

1. Introduction

Noctilucent clouds (NLC), also called *polar mesospheric clouds* (PMC), are made of water ice particles, which are sporadically observed by the naked eye at midlatitudes when these particles are illuminated by the Sun when it is several degrees below the horizon (Gadsden & Schröder, 1989). NLC can exist around the summer mesopause at middle and high latitudes since this region is extremely cold (130–140 K), actually being the coldest place in the Earth's atmosphere (Lübken, 1999). Some scientists claim that NLC are sensitive indicators for climate change due to a combination of cooling and/or an increase of water vapor (Hervig, Berger, & Siskind, 2016; Russell et al., 2015; Thomas, 1996, 2003; Thomas et al., 1989). This has been questioned because the database regarding long-term trends of NLC is still rather poor and too little is known about long-term trends and episodic changes of the background atmosphere at these altitudes (Thomas et al., 2003; von Zahn, 2003; von Zahn et al., 2004).

Observations in the upper mesosphere/lower thermosphere region are rather challenging. Very little is known about trends of basic parameters such as temperature and water vapor mixing ratio on centennial time scales. There is general consensus that an increase of greenhouse gases causes a cooling of the mesosphere due to an enhanced escape of infrared photons to space. There is one exception, however, namely, the summer mesopause region, where this effect is compensated for by increased absorption of photons from lower altitudes. Therefore, trends in this height region are very small (negative) or even positive (Berger & Lübken, 2011; Garcia et al., 2007; Marsh et al., 2013; Roble & Dickinson, 1989). Furthermore, it was shown recently that trends are not uniform in time but show episodic modulations (Lübken et al., 2013).

19448007, 2018, 13, Downloaded from https://agupubs.onlinelibrary.wiley.com/doi/10.1029/2018GL077719, Wiley Online Library on [05/11/2026]. See the Terms and Conditions (https://onlinelibrary.wiley.com/terms-and-conditions) on Wiley Online Library for rules of use; OA articles are governed by the applicable Creative Commons License

Modern technologies such as lidar and satellite-borne instruments have revealed many details about these clouds. The observational database on NLC/PMC including microphysical properties, variations with latitude and longitude, solar cycle, and tides has improved significantly in recent decades (see, e.g., Baumgarten et al., 2012; Fiedler et al., 2009; Gerding et al., 2013; Russell et al., 2015). Furthermore, there is increasing experimental and theoretical evidence that NLC/PMC occur more frequently in recent decades (Berger & Lübken, 2015; DeLand & Thomas, 2015; Hervig, Berger, & Siskind, 2016). However, the unequivocal detection of trends in NLC is still challenged due to the impact of various processes varying mainly in the last decades, for example, stratospheric ozone mixing ratios or water vapor transport through the tropical tropopause into the stratosphere (Brinkop et al., 2016; Lübken et al., 2013; Pertsev et al., 2014; WMO, 2011).

In the past we have performed model simulations of NLC at 69°/78°N and studied their long-term evolution concentrating on the period since 1961, that is, when ERA40 reanalysis data (since 1961) and satellite observations (since 1979) are available (Berger & Lübken, 2015; Berger & von Zahn, 2002; Lübken et al., 2009). In this paper we extend our studies to the time period 1871 to 2008 given by the availability of reanalysis data (see below for more details). We concentrate on the latitude band 55–61°N, that is, where NLC are visible by the naked eye. In the next section we describe the models being used in this paper. Model results of trends in the background atmosphere and in mesospheric ice layers as well as sensitivity studies are presented in section 3. The implications of our results for the role of anthropogenic activities on the morphology of NLC are discussed in section 4.

2. Method

The basic concept used in this paper is to model the background atmosphere with the Leibniz Institute Middle Atmosphere Model (LIMA) for northern hemispheric conditions in the time period from 1871 to 2008 and then use this background in the Mesospheric Ice Microphysics And tranSport (MIMAS) model to study mesospheric ice layers. In LIMA the mixing ratios of carbon dioxide (28–150 km) and ozone (28–65 km) are changing, whereas all other trace gases are kept constant. In MIMAS the water vapor mixing ratio is increasing with time, where this increase is based on the increase of methane in the troposphere and its contribution to the water vapor budget in the mesosphere (see below).

LIMA is a global model (0–150 km) taking into account major processes such as radiation, chemistry, and transport (Berger, 2008; Lübken et al., 2013). At lower heights (0–28 km) LIMA is nudged to the real atmosphere, namely, to twentieth century reanalysis data from NOAA-CIRES (National Oceanic and Atmospheric Administration-Cooperative Institute for Research in Environmental Sciences 20CR; Compo et al., 2011). In LIMA the effects of small-scale internal gravity waves are taken into account by a nonlinear spectral gravity wave parametrization (Yigit & Medvedev, 2013).

For CO_2 we use the monthly mean time series for the period 1961–2008 measured at Mauna Loa (19°N, 155°W). Before 1961 we use the historical CO_2 record derived from Antarctic ice cores (Etheridge et al., 1998). For ozone in the period 1961–2008 we take into account temporal and latitudinal variations in the stratosphere and lower mesosphere (Lübken et al., 2013; WMO, 2011). Before 1961 stratospheric ozone is kept constant with ozone values from the year 1961. LIMA and MIMAS use daily Lyman-α fluxes as a proxy for solar activity in the period from 1961 to 2008. Before 1961 Lyman-α values are approximated using monthly sunspot numbers.

The MIMAS ice model is a three-dimensional Lagrangian transport model specifically designed to study ice particles in the upper mesosphere (Berger & Lübken, 2015). MIMAS calculates ice layers in each NLC season from 10 May to 31 August and is limited to middle/polar latitudes (38°–90°N) and to the mesopause region (77.8–94 km). In MIMAS, 40 million dust/ice particles are transported according to three-dimensional and time-dependent background winds, eddy diffusion, and sedimentation. Ice particle nucleation and growth are described applying standard microphysical processes, including, for example, the Kelvin effect and the degree of saturation (Berger & Lübken, 2015; Gadsden & Schröder, 1989). Water vapor bound in ice particles and background water vapor are interactively coupled by freeze drying and sublimation.

The mixing ratio of H_2O in the mesosphere is basically given by two effects: (i) transport of H_2O from lower altitudes and (ii) oxidation of methane. We assume that the first contribution has not changed on centennial time scales, whereas variations in more recent decades are indeed likely (Hegglin et al., 2014). Even on decadal time scales there is no clear picture regarding trends of water vapor in the middle atmosphere

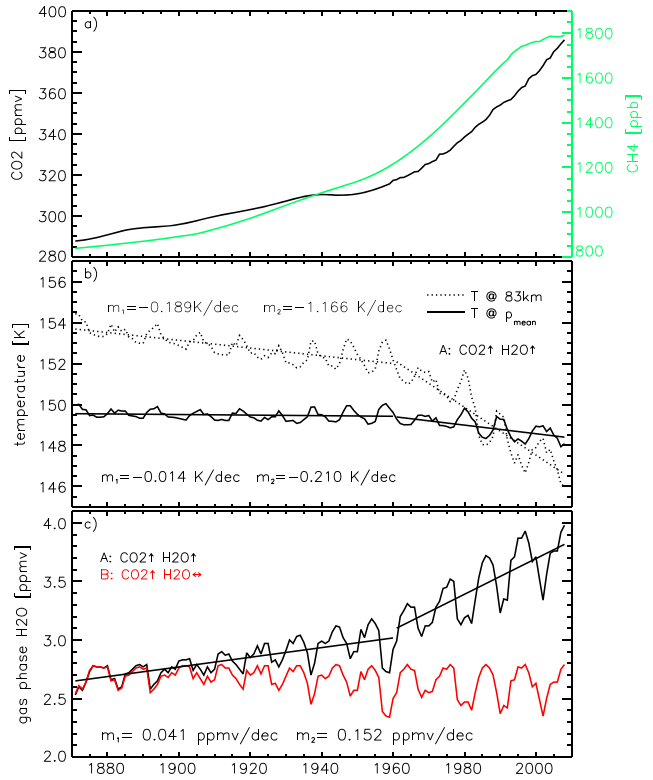


Figure 1. Time series of (a) tropospheric CO_2 (black line) and CH_4 (green line) mixing ratios from Mauna Loa observations and ice core data (Etheridge et al., 2002, 1998); (b) temperatures from Run A at a fixed geometric altitude (83 km) and at the mean pressure level of maximum backscatter (p_{mean}); (c) mixing ratios of gas phase water vapor at p_{mean} (assuming that ice formation had not occurred) for Runs A and B. Note that H_2O values for Runs A and C are identical. See text for more details on the definition of p_{mean}. In panels (b) and (c) linear fits for Run A are shown for the time periods before (m_1) and after (m_2) 1960, respectively. The slopes are listed in the inserted legend.

(see, e.g., Nedoluha et al., 2017). We have determined the relative contributions of the two sources of H_2O using recent satellite observations of H_2O and CH_4 from the instrument SOFIE (Solar Occulation For Ice Experiment) on the AIM satellite (Aeronomy of Ice in the Mesosphere) at the stratopause ($H_2O = 7.5$ ppmv and $CH_4^{50km} = 100$ ppbv; Rong et al., 2016). We also used tropospheric methane ($CH_4^{tropo} = 1{,}780$ ppmv) from other sources (Etheridge et al., 2002). This allows to determine the fraction of CH_4, which is converted to H_2O, namely, $\alpha = (CH_4^{tropo} - CH_4^{50km})/CH_4^{tropo} = 0.94$. In other words, at stratopause levels, 94% of methane entering the mesosphere has already been converted to water vapor. Since the oxidation of each methane molecule produces two water vapor molecules, we arrive at a H_2O mixing ratio due to CH_4 oxidation of $H_2O(CH_4) = 2 \cdot \alpha \cdot CH_4^{tropo} = 3.35$ ppmv at stratopause levels. This leaves H_2O(tropo) = 7.5 − 3.35 = 4.15 ppmv originating from direct transport from the troposphere. We use these considerations to estimate the long-term evolution of H_2O in the mesosphere, namely, keeping H_2O(tropo) = 4.15 ppmv constant and adding $H_2O(CH_4)$ using long-term changes in CH_4^{50km} (Dlugokencky et al., 2015; Etheridge et al., 2002). Furthermore, we take into account that in the upper mesosphere some of the water vapor is destroyed by photodissociation.

Very little is known about potential long-term effects of winds and wave activity on the mean circulation. Since any consideration of potential long-term effects would be highly speculative, we decided to use a particular dynamical situation (winds, wave activity, and variability in background winds) from a representative year, namely, 1982, for all years 1971 − 2008. However, the conclusions are not dependent on the choice of year. Thereby, a potential impact of trends in mean background winds and wave activity on NLC trends is eliminated.

3. Results

3.1. Trends in Atmospheric Background

In Figure 1a we show the long-term evolution of CO_2 and CH_4 mixing ratios used in this study. Both time series show an accelerated increase after approximately 1960. We have performed model runs for the following scenarios: (A) CO_2 increasing, H_2O increasing (CO_2 ↑,H_2O↑); (B) CO_2 increasing, H_2O constant, where the value is taken from 1880 (CO_2 ↑,H_2O↔); and (C) CO_2 and O_3 constant with value from 1880, H_2O increasing (CO_2 ↔,H_2O↑). We average over the core of the summer season, namely, July.

In Figure 1b we show time series for Run A of temperatures at NLC altitudes, more precisely at a fixed altitude, namely, at 83 km, and also at a fixed pressure $p_{mean} = 5.962 \cdot 10^{-3}$ hPa (same for all years) where this pressure is given by the average of all 138 mean pressure levels of maximum backscatter. Figure 1b demonstrates the difference between temperature trends at geometric altitudes and at fixed pressure levels. We show temperatures for Run A only since they are identical to Run B because the time series for CO_2 and O_3 are identical in both runs. Temperatures in Run C are constant since CO_2 and O_3 are constant and the H_2O change takes place in MIMAS and therefore does not modify background temperatures. Temperatures at 83 km have decreased by ~7 K since 1871, whereas they are rather constant at the pressure level p_{mean}. The reason for this difference is that the atmosphere in the lower and middle mesosphere shrinks because of cooling. This implies that a given pressure level is shifted to lower geometric heights. Due to the negative temperature lapse rate at NLC altitudes, the downward shift of the temperature profile leads to an apparent cooling at fixed geometric altitudes. As can be seen in Figure 1b the temperature decrease at 83 km is not monotonous in time but is accelerated after approximately 1960, following the CO_2 time series shown in Figure 1a. We have therefore determined linear trends before and after 1960, respectively, and arrive at slopes of $m_1 = -0.189$ and $m_2 = -1.166$ K/decade in the time periods 1871 − 1960 and 1960 − 2008, respectively. This means that temperature trends are more than a factor of 6 larger in recent decades compared to the beginning of industrialization. Marsh et al. (2013) have recently published model trend results and arrive at a total difference between preindustrial and modern

19448007, 2018, 13, Downloaded from https://agupubs.onlinelibrary.wiley.com/doi/10.1029/2018GL077719, Wiley Online Library on [05/11/2026]. See the Terms and Conditions (https://onlinelibrary.wiley.com/terms-and-conditions) on Wiley Online Library for rules of use; OA articles are governed by the applicable Creative Commons License

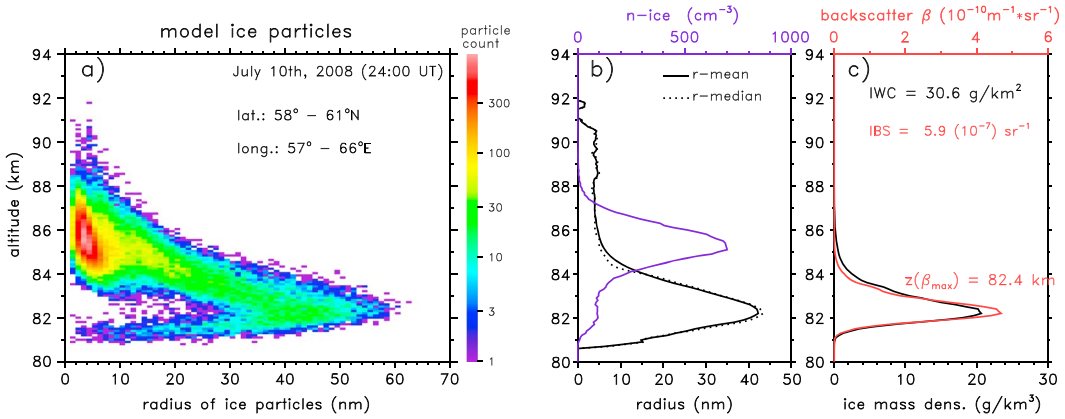


Figure 2. Example of ice layer characteristics of an NLC: (a) 2-D histogram of number of ice particles in the given latitude and longitude bin per $\Delta z = 100$ m and $\Delta r = 1$ nm (*counts*) as a function of altitude and particle radius; (b) mean and median radius of ice particles (black lines, lower *x* axis), and ice particle number density (blue line, upper *x* axis); and (c) ice mass density (black line, lower *x* axis) and backscatter coefficient (red line, upper panel). The inserted legend gives the altitude of maximum backscatter, $z(\beta_{max})$, the integrated backscatter (IBS), and the ice water content (IWC).

temperatures of about −2 K at NLC pressure levels (see Figure 9b in their paper). This is comparable to the total temperature change (T @ p_{mean}) shown in Figure 1b. Note that the maximum backscatter β_{max} is nearly colocated with the lower altitude where the degree of saturation equals 1 since particles grow above this height where $S > 1$. This implies that the temperatures given in Figure 1b labeled T @ p_{mean} are practically identical to frost point temperatures (the difference is less than 1 K).

We have determined temperature trends in the entire mesosphere and lower thermosphere (not shown). Temperature trends since 1960 are rather large in the middle mesosphere (up to −1.5 K/decade) but are small around NLC pressure levels. In this study the long-term cooling is entirely due to an increase of CO_2 and varying O_3. The total cooling since 1871 amounts to approximately 10 K in the middle mesosphere but is much smaller at NLC pressure levels and close to 0 at the mesopause. Water vapor mixing ratios at p_{mean} are shown in Figure 1c. We depict H_2O mixing ratios for the hypothetical case that no ice formation had occurred. Note that H_2O values for Runs A and C are identical. The mixing ratio of water vapor increases by ∼0.15 ppmv/decade since 1960 (Runs A and C). The total increase is about 40% since 1871 (approximately 1 ppmv), which in this study is entirely caused by the increase of methane oxidizing to H_2O.

In Figure 2 we show an example of ice cloud parameters within a spatial section of 3 longitude bins of 3° each (out of 120) and 3 latitude bins of 1° each (out of 53). We show the altitude distribution of particle radii, number densities, ice mass density, and backscatter coefficients (β) for a wavelength of $\lambda = 532$ nm, which is often used by lidars detecting NLC (see, e.g., Collins et al., 2009; Fiedler et al., 2009). From this we determine the maximum backscatter (β_{max}), the altitude of this maximum z(β_{max}), the height integrated value of β (integrated backscatter), and the total amount of ice mass in a column (ice water content, IWC). Throughout this paper β and β_{max} are given in units of 10^{-10} m/sr, and IWC in g/km^2. For simplicity we term the altitude of β_{max} *NLC altitude*. In order to account for the limited sensitivity of a visual observer watching NLC, we occasionally limit our analysis to clouds with a threshold for β_{max}. In this paper we use $\beta_{max} > 3$ as a typical limit for visible NLC (Baumgarten et al., 2009).

3.2. Trends in Mesospheric Ice Layers

In Figure 3 we show the temporal development of various ice layer parameters. The information from a total of about one quadrillion (10^{15}) dust and ice particles in MIMAS enters into the values shown in this plot. Mean NLC altitudes with $\beta_{max} > 3$ (Figure 3a) have decreased by approximately 1.3 km from 1871 to 2008, where the major part of this decline occurs after ∼1960. The decrease occurs only when CO_2 increases (Runs A and B), which is due to the fact that the lower height limit of supersaturation decreases when the atmosphere shrinks (see above). Water vapor alone (Run C) does not change NLC altitudes significantly. To indicate the vertical extent of the NLC layer, we also show the lower edge of the ice layer (for Run A), which is located about 1.6 km below the peak of the layer. Note that the difference between the peak and the lower edge of the NLC layers is practically independent of time.

19448007, 2018, 13, Downloaded from https://agupubs.onlinelibrary.wiley.com/doi/10.1029/2018GL077719, Wiley Online Library on [05/11/2026]. See the Terms and Conditions (https://onlinelibrary.wiley.com/terms-and-conditions) on Wiley Online Library for rules of use; OA articles are governed by the applicable Creative Commons License

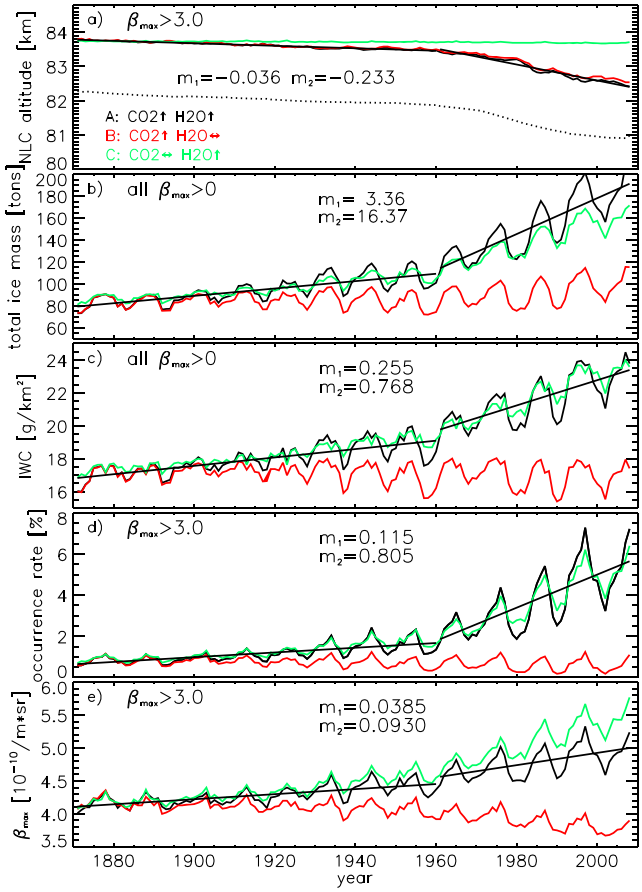


Figure 3. Time series of monthly mean values in the latitude band 55°–61°N of (a) NLC altitude (solid) and lower edge (dotted); (b) total ice mass; (c) ice water content (IWC); (d) occurrence rate for NLC; and (e) maximum backscatter. Results from the three runs (A, B, and C) are shown (black, red, and green lines). In panels (a), (d), and (e) a threshold of $\beta_{max} > 3$ is applied. Slopes for the time periods before (m_1) and after (m_2) 1960 are also shown (black lines). The slopes are listed in the inserted legend. Units of m_1 and m_2 are [...] per decade where [...] are the units shown on the *y* axis. NLC = noctilucent cloud.

The total ice mass (M_{ice}) in the latitude range 55°–61°N has increased from approximately 80 to 180 tons; that is, it has more than doubled in the period 1871 to 2008 (Figure 3b, Runs A and C). The ice mass increases mainly if H_2O mixing ratio is increasing (Runs A and C), whereas a temperature decrease alone (Run B) has a much smaller effect. Most of the ice mass increase has occurred after approximately 1960. Water vapor increase alone (Run C) increases the total ice mass by ~72 tons, whereas temperature decrease only (Run B) increases the total ice mass by approximately 17 tons (all numbers averaged over a solar cycle). The latter is due to the fact that cooling enhances the chance for ice particles to be generated. The combination of H_2O increase and cooling due to CO_2 increase (Run A) enhances M_{ice} by ~100 tons. This implies that an increase of water vapor has the largest effect on the total ice mass, whereas the impact of temperature decrease is much smaller. We note that the situation may be different at higher latitudes.

In Figure 3d we show the occurrence rates of NLC, which are determined as follows: the maximum possible number of NLC events is given by the number of latitude bins (6), longitude bins (120), and time slots of 6 hr each (=31 days × 4 per day = 124 time slots), which totals to 89,280 events per season. This is compared to the number of NLC events actually being present, applying a given threshold. In Figure 3d we show occurrence rates for a threshold of $\beta_{max} > 3$. The occurrence rates increase from approximately 1% to 6% from 1871 to 2008, respectively. We will discuss the sensitivity of this increase on the threshold for β_{max} in section 3.3. The IWC increase shown in Figure 3c is less pronounced compared to the increase of total ice mass. This difference is explained as follows. For a given year the mean IWC is defined as the mean over all bins filled with NLC, whereas the total ice mass is the sum of all ice masses in all bins filled with NLC. Since the occurrence rates (i.e., the number of bins filled with NLC) increase with time, the total ice mass increases more rapidly compared to the mean IWC.

As can be seen in Figure 3e β_{max} also increases significantly when more H_2O is available (Runs A and C), whereas cooling alone (i.e., increase of CO_2, Run B) surprisingly leads to a slight reduction of β_{max}. The reason for this is that smaller (but more) ice particles are generated when temperatures are reduced. Smaller particles in turn cause less scattering of light eventually falling below the threshold imposed on β_{max}. We note that some ice parameters show a substantial modulation with solar cycle, which is mainly given by photodissociation of water vapor varying with solar activity.

3.3. Sensitivities

We have studied the sensitivity of the temporal development of ice layer parameters on the threshold of β_{max}. Such a threshold is imposed, for example, by observers who can only see NLC exceeding a certain brightness. We have averaged ice layer parameters for two time periods with a duration of 11 years each (one solar cycle), namely, at the beginning (1871–1881) and at the end (1998–2008) of the total time interval, respectively. In Figure 4a we show occurrence rates as a function of a threshold for β_{max}. If we consider, for example, the time period 1998–2008 and a threshold of $\beta_{max} > 3$, we arrive at 4,525 cases of NLC per season (in the mean), which corresponds to an occurrence rate of 4,525/89,280 or 5.1%. For a visual observer at a fixed location the number of cases are reduced further by a factor of approximately 5.5×10^{-4}, which is given by the limited observation time (typically ~2 hr per day = 2/24 hr), the limited longitude coverage (typically 4/360°), and the limited chance for clear sky conditions (roughly 40%). This implies that 1–2 NLC events per season correspond to an occurrence frequency of roughly $100/(89280 \cdot 5.5 \cdot 10^{-4})$~2–4%. For $\beta_{max} > 3$ the occurrence rate is 5% in recent times, whereas it was only 0.8% at the end of the nineteenth century (Figure 4a). Note that the difference in the mean probability of observing an NLC in the periods 1871–1881 and 1998–2008, respectively,

19448007, 2018, 13, Downloaded from https://agupubs.onlinelibrary.wiley.com/doi/10.1029/2018GL077719, Wiley Online Library on [05/11/2026]. See the Terms and Conditions (https://onlinelibrary.wiley.com/terms-and-conditions) on Wiley Online Library for rules of use; OA articles are governed by the applicable Creative Commons License

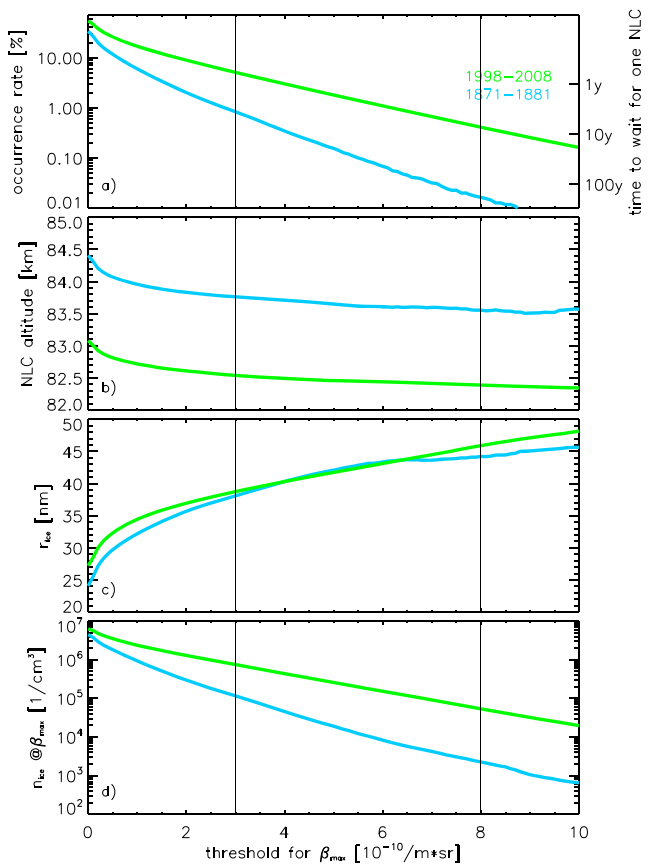


Figure 4. NLC parameters as a function of the sensitivity to detect ice layers, that is, of the threshold for β_{max}, for two time periods of one solar cycle each, namely, at the beginning (1871–1881, blue lines) and at the end (1998–2008, green lines) of the total time period. (a) Occurrence rate and the average time required to detect an NLC (see text for more details); (b) mean NLC altitude; (c) mean ice particle radius at β_{max}; and (d) total number of ice particles per unit volume at β_{max}. All results are from Run A (CO_2 and H_2O increasing). NLC = noctilucent cloud.

increases if the threshold increases. For example, the chance to observe a bright NLC ($\beta_{max} > 8$) is still reasonable in current times (some in a few years), whereas it was extremely unlikely before the twentieth century (one NLC per several hundred years, see Figure 4a).

NLC altitudes shown in Figure 4b do not change significantly for $\beta_{max} > 3$ if the threshold is increased. Note that NLC were located about 1.2 km higher before the industrialization compared to recent times. This height difference is rather independent of the threshold being applied. We discuss NLC altitudes in more detail in the next section. The sensitivity of seasonal mean ice particle radii, r_{ice}, at β_{max} is shown in Figure 4c. As expected, r_{ice} increases with increasing threshold, because brighter NLC require larger ice particles. This also explains why the behavior of r_{ice} as a function of the threshold is rather similar for both time periods. The total number of ice particles per unit volume at β_{max} decreases rapidly when the threshold of β_{max} increases (Figure 4d). This reflects the fact that there are fewer *large* and more *small* ice particles in the ice cloud (see Figure 2a). Generally speaking, there were far fewer ice particles in the NLC layer at the beginning of the industrialization compared to today. We note that mean parameters representing the background atmosphere and also ice layer characteristics are associated with some natural variability.

4. Discussion and Conclusion

Mesospheric temperature trends in LIMA are consistent with temperature trend observations from lidar. For example, in the period 1979–1997 during summer near 45°N large cooling trends of about −3 K/decade are observed, which reduce and even turn to warming around mesopause heights (see Figure 10 in Keckhut et al., 2011). This is in nice agreement with LIMA results (see Figure 1b in Berger & Lübken, 2011). The associated descent rate of NLC heights is consistent with long-term observations of radio wave reflection heights performed since 1959 (see Figure 2a in Berger & Lübken, 2011). The H_2O mixing ratio in recent years (~4 ppmv, see Figure 1c, Run A) agrees nicely with contemporary satellite observations by SOFIE/AIM (Figure 6d in Hervig, Gerding, et al., 2016). Only very few studies on water vapor trends in the summer mesopause region at middle latitudes are available (see, e.g., Hervig, Berger, & Siskind, 2016; Remsberg et al., 2018). The latest is from Remsberg et al. (2018), which shows a water vapor trend of approximately 5%/decade at 52.5°N and 80 km corresponding to ~0.175 ppmv/decade, which is consistent with the trends shown in Figure 1c (~0.15 ppmv/decade). Unfortunately, no information is available on long-term evolution of temperatures or water vapor in the upper mesosphere on centennial time scales.

Ice particle radii from MIMAS (Figure 4c) are generally consistent with lidar observations at 54°N (Alpers et al., 2000). Regarding IWC, the instrument SOFIE/AIM measured a mean of IWC ~ 59 at midlatitudes during July 2015, applying a threshold of IWC > 40 (see Figure 3 in Hervig, Gerding, et al., 2016). This is in perfect agreement with IWC values from LIMA at the end of our time period (2008), namely, IWC ~ 58–59, applying the same threshold.

It is rather challenging to determine uncertainties of the yearly mean background and ice parameters discussed in this paper. We decided to concentrate on uncertainties regarding the derivation of mesospheric water vapor in MIMAS, more precisely on the parameter α (see section 2). Rong et al. (2016) have compared SOFIE/AIM observations with measurements from other satellites. For the summer season in the Northern Hemisphere they arrive at a mean of approximately $CH_4^{50km} = 100$ ppbv around the stratopause (the value used in this paper) with a typical uncertainty of ±50 ppbv (see Figure 5 in their paper). This corresponds to an uncertainty of approximately ±3% in α and ±2% in H_2O.

19448007, 2018, 13, Downloaded from https://agupubs.onlinelibrary.wiley.com/doi/10.1029/2018GL077719, Wiley Online Library on [05/11/2026]. See the Terms and Conditions (https://onlinelibrary.wiley.com/terms-and-conditions) on Wiley Online Library for rules of use; OA articles are governed by the applicable Creative Commons License

19448007, 2018, 13, Downloaded from https://agupubs.onlinelibrary.wiley.com/doi/10.1029/2018GL077719, Wiley Online Library on [05/11/2026]. See the Terms and Conditions (https://onlinelibrary.wiley.com/terms-and-conditions) on Wiley Online Library for rules of use; OA articles are governed by the applicable Creative Commons License

Former investigations on the relevance of NLC for the detection of climate change have concentrated on idealized sensitivity studies of mesospheric ice layers on temperature and H_2O (Bardeen et al., 2010; Hervig et al., 2009; Lübken et al., 2007; Rong et al., 2012; Thomas et al., 1989; von Zahn & Berger, 2003). In this paper we model temperatures and water vapor trends in the mesosphere for long time periods (1871–2008) based on tropospheric and lower stratospheric reanalysis data. This allows to derive all relevant ice layer parameters from the development of individual ice particles and to compare with contemporary observations. Note that trend studies covering the last few decades are hampered by the fact that anthropogenic activities have modified some parameters in this period, which were presumably constant before, for example, stratospheric ozone or H_2O injection into the stratosphere (Brinkop et al., 2016).

The first detection of NLC was reported in 1885 (e.g., Backhouse, 1885). A more quantitative study of NLC from the years 1889–1891 provided a mean altitude of 82.08 km (Jesse, 1896). The mean NLC altitude from LIMA/MIMAS in the late nineteenth century is somewhat higher (~83.8 km, see Figure 3a). Apart from the limited historical data base there are several reasons that can explain this difference. For example, (i) the variability of NLC altitudes in LIMA/MIMAS is approximately 0.6 km (2σ value) for $\beta > 3$, (ii) the triangulation of structures within an NLC leads to altitudes significantly lower than the height of β_{max} (Ridder et al., 2017), and (iii) the influence of tides may cause a systematic bias for NLC altitudes for an observer detecting at a fixed local time (Fiedler et al., 2005; Gerding et al., 2013).

The question remains why NLC were not reported before 1885. We follow the reasonable speculation presented by Thomas et al. (1989), namely, that the first observation was triggered by the eruption of Krakatoa, which ejected millions of tons of H_2O into the stratosphere. For a given increase of H_2O mixing ratio we can easily estimate the increase of ice mass, integrated backscatter, and β_{max}, given the results presented in this paper. We find that the water increase suggested by Thomas et al. (1989) would lead to NLC with a brightness of approximately β_{max} ~6.5, that is, bright shining clouds. We will investigate the role of volcanic eruptions for the long-term evolution of NLC in more detail in the future.

We conclude that the rise of H_2O concentration due to increasing CH_4 has lead to a large enhancement of the visibility of clouds, in particular, since the 1960s. The anthropogenic increase of CO_2 leads to a large cooling in the middle and lower mesosphere but less so at NLC heights. To first order this cooling leads to a small increase of total ice mass but has little impact on the visibility of ice clouds since smaller (but more) ice particles are generated, which create too little scattering. Roughly speaking, temperatures must be low enough to allow for ice nucleation, but the visibility of ice clouds is primarily determined by the amount of water vapor available for ice particle growth.

Cooling in the mesosphere decreases the height of NLC due to atmospheric shrinking, whereas an increase of H_2O alone has little effect on the mean NLC altitude. Note that this study concentrates on middle latitudes and that results at high latitudes might be different. In recent decades it is likely to see one or more NLC per season, whereas the probability was only once per several decades before the beginning of industrialization. The chance to see an NLC decreases exponentially with brightness, as shown in this paper. Therefore, the probability was even smaller for very bright NLC, namely, one per several centuries. NLC were too infrequent and too unspectacular in historical times to be identified as a unique phenomenon.

We conclude that NLC are indeed a long-term indicator for climate change due to the increase of H_2O caused by the oxidation of methane, whereas the growth of carbon dioxide mixing ratio is of secondary importance. Episodic changes of H_2O and O_3 as well as other factors may impact the morphology of NLC on decadal time scales.

Acknowledgments
We are grateful for the twentieth century reanalysis data from NOAA-CIRES supported by the DOE-INCITE, BER, and NOAA program and also for the SBUV Merged Ozone Data Set from https://acd-ext.gsfc.nasa.gov/Data-services/merged/. Lyman-α data are available at http://lasp.colorado.edu/lisird/lya/ from LASP. Sunspot data are provided by the World Data Center SILSO. We acknowledge the Mauna Loa records for CO_2 and CH_4 from http://www.esrl.noaa.gov/gmd/ccgg/ and ftp://ftp.cmdl.noaa.gov/ccg/ch4/in-situ/. Historical CH_4 records are from http://cdiac.ess-dive.lbl.gov/trends/atm_meth/lawdome_meth.html. Data in this paper are available at ftp://ftp.iap-kborn.de/data-in-publications/LuebkenGRL2018/ We appreciate the financial support from the German BMBF project TIMA, which is part of the ROMIC program.

References

Alpers, M., Gerding, M., Höffner, J., & von Zahn, U. (2000). NLC particle properties from a five-color observation at 54°N. *Journal of Geophysical Research*, *105*, 12,235–12,240.

Backhouse, T. W. (1885). The luminous cirrus cloud of June and July. *Meteorological Magazine*, *20*, 133.

Bardeen, C. G., Toon, O. B., Jensen, E. J., Hervig, M. E., Randall, C. E., Benze, S., et al. (2010). Numerical simulations of the three-dimensional distribution of polar mesospheric clouds and comparisons with Cloud Imaging and Particle size (CIPS) experiment and the Solar Occultation For Ice Experiment (SOFIE) observations. *Journal of Geophysical Research*, *115*, D10204. https://doi.org/10.1029/2009JD012451

Baumgarten, G., Chandran, A., Fiedler, J., Hoffmann, P., KaiflerN, N., Lumpe, J., et al. (2012). On the horizontal and temporal structure of noctilucent clouds as observed by satellite and lidar at ALOMAR (69°N). *Geophysical Research Letters*, *39*, L01803. https://doi.org/10.1029/2011GL049935

Baumgarten, G., Fiedler, J., Fricke, K. H., Gerding, M., Hervig, M., Hoffmann, P., et al. (2009). The noctilucent cloud (NLC) display during the ECOMA/MASS sounding rocket flights on 3 August 2007: Morphology on global to local scales. *Annales de Geophysique*, *27*, 953–965.

Berger, U. (2008). Modeling of middle atmosphere dynamics with LIMA. *Journal of Atmospheric and Solar-Terrestrial Physics*, *70*, 1170–1200. https://doi.org/10.1016/j.jastp.2008.02.004

Berger, U., & Lübken, F.-J. (2011). Mesospheric temperature trends at mid-latitudes in summer. *Geophysical Research Letters*, *38*, L22804. https://doi.org/10.1029/2011GL049528

Berger, U., & Lübken, F.-J. (2015). Trends in mesospheric ice layers in the Northern Hemisphere during 1961–2013. *Journal of Geophysical Research: Atmospheres*, *120*, 11,277–11,298. https://doi.org/10.1002/2015JD023355

Berger, U., & von Zahn, U. (2002). Icy particles in the summer mesopause region: Three-dimensional modeling of their environment and two-dimensional modeling of their transport. *Journal of Geophysical Research*, *107*(A11), 1366. https://doi.org/10.1029/2001JA000316

Brinkop, S., Dameris, M., Jöckel, P., Garny, H., Lossow, S., & Stiller, G. (2016). The millennium water vapour drop in chemistry–climate model simulations. *Atmospheric Chemistry and Physics*, *16*, 8125–8140. https://doi.org/10.5194/acp-16-8125-2016

Collins, R. L., Taylor, M. J., Nielsen, K., Mizutani, K., Murayama, Y., Sakanoi, K., & DeLand, M. T. (2009). Noctilucent cloud in the western Arctic in 2005: Simultaneous lidar and camera observations and analysis. *Journal of Atmospheric and Solar-Terrestrial Physics*, 446–452. https://doi.org/10.1016/j.jastp.2008.09.044

Compo, G. P., Whitaker, J. S., Sardeshmukh, P. D., Matsui, N., Allan, R. J., Yin, J. X., et al. (2011). The twentieth century reanalysis project. *Quarterly Journal of the Royal Meteorological Society*, *137*, 1–28. https://doi.org/10.1002/qj.776

DeLand, M. T., & Thomas, G. E. (2015). Update PMC trends derived from SBUV data. *Journal of Geophysical Research: Atmospheres*, *120*, 2140–2166. https://doi.org/10.1002/2014JD022253

Dlugokencky, E. J., Crotwell, A., Lang, P., & Masarie, K. (2015). Atmospheric methane dry air mole fractions from quasi-continuous measurements at Barrow, Alaska and Mauna Loa, Hawaii, 1986-2014, version: 2015-04-28. Retrieved from ftp://ftp.cmdl.noaa.gov/ccg/ch4/in-situ/

Etheridge, D. M., Steele, L. P., Francey, R. J., & Langenfelds, R. L. (2002). Historical CH_4 records since about 1000 A.D. from ice core data. In *Trends: A compendium of data on global change*. Oak Ridge, TN: Carbon Dioxide Information Analysis Center, Oak Ridge National Laboratory, U.S. Department of Energy.

Etheridge, D., Steele, L., Langenfelds, R., Francey, R., Barnola, J.-M., & Morgan, V. (1998). Historical CO_2 records from the Law Dome DE08, DE08-2, and DSS ice cores. In *Trends: A compendium of data on global change, Carbon Dioxide Information Analysis Center*. Oak Ridge, TN: Oak Ridge National Laboratory, U.S. Department of Energy.

Fiedler, J., Baumgarten, G., & Lübken, F.-J. (2009). NLC observations during one solar cycle above ALOMAR. *Journal of Atmospheric and Solar-Terrestrial Physics*, *71*, 424–433. https://doi.org/10.1016/j.jastp.2008.11.010

Fiedler, J., Baumgarten, G., & von Cossart, G. (2005). Mean diurnal variations of noctilucent clouds during 7 years of lidar observations at ALOMAR. *Annales de Geophysique*, *23*, 1175–1181.

Gadsden, M., & Schröder, W. (1989). *Noctilucent clouds*. New York: Springer-Verlag.

Garcia, R. R., Marsh, D. R., Kinnson, D. E., Boville, B. A., & Sassi, F. (2007). Simulation of secular trends in the middle atmosphere, 1950–2003. *Journal of Geophysical Research*, *112*, D09301. https://doi.org/10.1029/2006JD007485

Gerding, M., Höffner, J., Hoffmann, P., Kopp, M., & Lübken, F.-J. (2013). Noctilucent cloud variability and mean parameters from 15 years of lidar observations at a mid-latitude site (54°N, 12°E). *Journal of Geophysical Research: Atmospheres*, *118*, 317–328. https://doi.org/10.1029/2012JD018319

Hegglin, M. I., Plummer, D. A., Shepherd, T. G., Scinocca, J. F., Anderson, J., Froidevaux, L., et al. (2014). Vertical structure of stratospheric water vapour trends derived from merged satellite data. *Nature Geoscience*, *7*, 768–776. https://doi.org/10.1038/ngeo2236

Hervig, M. E., Berger, U., & Siskind, D. E. (2016). Decadal variability in PMCs and implications for changing temperature and water vapor in the upper mesosphere. *Journal of Geophysical Research: Atmospheres*, *121*, 2383–2392. https://doi.org/10.1002/2015JD024439

Hervig, M. E., Gerding, M., Stevens, M. H., Stockwell, R., Bailey, S. M., Russell, J. M. III, & Stober, G. (2016). Mid-latitude mesospheric clouds and their environment from SOFIE observations. *Journal of Atmospheric and Solar-Terrestrial Physics*, *149*, 1–14. https://doi.org/10.1016/j.jastp.2016.09.004

Hervig, M. E., Stevens, M. H., Gordley, L. L., Deaver, L. E., Russell, J. M. III, & Bailey, S. M. (2009). Relationships between polar mesospheric clouds, temperature, and water vapor from Solar Occultation for Ice Experiment (SOFIE) observations. *Journal of Geophysical Research*, *114*, D20203. https://doi.org/10.1029/2009JD012302

Jesse, O. (1896). Die Höhe der leuchtenden Nachtwolken. *Astronomische Nachrichten*, *140*, 161–168.

Keckhut, P., Randel, W. J., Claud, C., Leblanc, T., Steinbrecht, W., Funatsu, B. M., et al. (2011). An evaluation of uncertainties in monitoring middle atmosphere temperatures with the ground-based lidar network in support of space observations. *Journal of Atmospheric and Solar-Terrestrial Physics*, 73, 627–642. https://doi.org/10.1016/j.jastp.2011.01.003

Lübken, F.-J. (1999). Thermal structure of the Arctic summer mesosphere. *Journal of Geophysical Research*, *104*(D8), 9135–9149.

Lübken, F.-J., Berger, U., & Baumgarten, G. (2009). Stratospheric and solar cycle effects on long-term variability of mesospheric ice clouds. *Journal of Geophysical Research*, *114*, D00106. https://doi.org/10.1029/2009JD012377

Lübken, F.-J., Berger, U., & Baumgarten, G. (2013). Temperature trends in the midlatitude summer mesosphere. *Journal of Geophysical Research: Atmospheres*, *118*, 13,347–13,360. https://doi.org/10.1002/2013JD020576

Lübken, F.-J., Rapp, M., & Strelnikova, I. (2007). The sensitivity of mesospheric ice layers to atmospheric background temperatures and water vapor. *Advances in Space Research*, *40*, 794–801. https://doi.org/10.1016/j.asr.2007. 01.014

Marsh, D. R., Mills, M. J., Kinnison, D. E., Lamarque, J.-F., Calvo, N., & Polvani, L. M. (2013). Climate change from 1850 to 2005 simulated in CESM1(WACCM). *Journal of Climate*, *26*, 7372–7390. https://doi.org/10.1175/JCLI-D-12-00558.1

Nedoluha, G., Kiefer2, M., Lossow, S., Gomez, R., Kämpfer, N., Lainer, M., et al. (2017). The SPARC water vapor assessment II: Intercomparison of satellite and ground-based microwave measurements. *Atmospheric Chemistry and Physics*, *17*, 14,543–14,558. https://doi.org/10.5194/acp-17-14543-2017

Pertsev, N., Dalin, P., Perminov, V., Romejko, V., Dubietis, A., Balčiunas, R., et al. (2014). Noctilucent clouds observed from the ground: Sensitivity to mesospheric parameters and long-term time series. *Earth Planets Space*, *66*(98), 1–9.

Remsberg, E., Damadeo, R., Natarajan, M., & Bhatt, P. (2018). Observed responses of mesospheric water vapor to solar cycle and dynamical forcings. *Journal of Geophysical Research: Atmospheres*, *123*, 3830–3843. https://doi.org/10.1002/2017JD028029

Ridder, C., Baumgarten, G., Fiedler, J., Lübken, F.-J., & Stober, G. (2017). Analysis of small-scale structures in lidar observations of noctilucent clouds. *Journal of Atmospheric and Solar-Terrestrial Physics*, *162*, 48–56. https://doi.org/10.1016/j.jastp.2017.04.005

Roble, R. G., & Dickinson, R. E. (1989). How will changes in carbon dioxide and methane modify the mean structure of the mesosphere and thermosphere? *Geophysical Research Letters*, *16*(12), 1441–1444.

19448007, 2018, 13, Downloaded from https://agupubs.onlinelibrary.wiley.com/doi/10.1029/2018GL077719, Wiley Online Library on [05/11/2026]. See the Terms and Conditions (https://onlinelibrary.wiley.com/terms-and-conditions) on Wiley Online Library for rules of use; OA articles are governed by the applicable Creative Commons License

Rong, P. P., Russell, J. M. III, Hervig, M. E., & Bailey, S. M. (2012). The roles of temperature and water vapor at different stages of the polar mesospheric cloud season. *Journal of Geophysical Research*, *117*, D04208. https://doi.org/10.1029/2011JD016464

Rong, P. P., Russell, J. M. III, Marshall, B. T., Siskind, D. E., Hervig, M. E., Gordley, L. L., et al. (2016). Version 1.3 AIM SOFIE measured methane (CH_4): Validation and seasonal climatology. *Journal of Geophysical Research: Atmospheres*, *121*, 13,158–13,179. https://doi.org/10.1002/2016JD025415

Russell, J. M. III, Rong, P., Hervig, M. E., Siskind, D. E., Stevens, M. H., Bailey, S. M., & Gumbel, J. (2015). Analysis of northern midlatitude noctilucent cloud occurrences using satellite data and modeling. *Journal of Geophysical Research: Atmospheres*, *119*, 3238–3250. https://doi.org/10.1002/2013JD021017

Thomas, G. (1996). Is the polar mesosphere the miner's canary of global change? *Advances in Space Research*, *18*(3), 149–158.

Thomas, G. E. (2003). Are noctilucent clouds harbingers of global change in the middle atmosphere? *Advances in Space Research*, *32*, 1737–1746.

Thomas, G., Olivero, J., DeLand, M., & Shettle, E. (2003). Comment on "Are noctilucent clouds truly a "Miner's Canary" for Global Change?" *Eos, Transactions American Geophysical Union*, *84*(36), 352–353.

Thomas, G. E., Olivero, J. J., Jensen, E. J., Schröder, W., & Toon, O. B. (1989). Relation between increasing methane and the presence of ice clouds at the mesopause. *Nature*, *338*, 490–492.

von Zahn, U. (2003). Are noctilucent clouds truly a "Miner's Canary" for global change? *Eos, Transactions American Geophysical Union*, *84*(28), 261–264.

von Zahn, U., Baumgarten, G., Berger, U., Fiedler, J., & Hartogh, P. (2004). Noctilucent clouds and the mesospheric water vapour: The past decade. *Atmospheric Chemistry and Physics*, *4*, 2449–2464.

von Zahn, U., & Berger, U. (2003). Persistent ice cloud in the midsummer upper mesosphere at high latitudes: Three-dimensional modeling and cloud interactions with ambient water vapor. *Journal of Geophysical Research*, *108*(D8), 8451. https://doi.org/10.1029/2002JD002409

WMO (2011). *WMO World Meteorological Organization: Global ozone research and monitoring project—Report No. 52, Chapter 2*. Geneva, Switzerland: Stratospheric Ozone and Surface Ultraviolet Radiation.

Yigit, E., & Medvedev, A. (2013). Extending the parameterization of gravity waves into the thermosphere and modelling their effects. In F.-J. Lübken (Ed.), *Climate and weather of the Sun-Earth system (CAWSES): Highlights from a priority program* (25 pp.). Dordrecht, Netherlands: Springer. https://doi.org/10.1007/978-94-007-4348-9-25

19448007, 2018, 13, Downloaded from https://agupubs.onlinelibrary.wiley.com/doi/10.1029/2018GL077719, Wiley Online Library on [05/11/2026]. See the Terms and Conditions (https://onlinelibrary.wiley.com/terms-and-conditions) on Wiley Online Library for rules of use; OA articles are governed by the applicable Creative Commons License